
ACCELERATING MATERIALS DISCOVERY USING FOUNDATION MODEL BASED IN-CONTEXT ACTIVE LEARNING *

Jeffrey Hu¹, Rongzhi Dong², Ying Feng³, Ming Hu⁴, Jianjun Hu^{2†}

¹Department of Materials Science and Engineering, University of Illinois Urbana Champaign, Champaign, IL, USA

²Department of Computer Science & Engineering, University of South Carolina, Columbia, USA

³Zuoyue Honors College, Hangzhou Dianzi University, Hangzhou, China

⁴Department of Mechanical Engineering, University of South Carolina, Columbia, USA

ABSTRACT

Active learning (AL) has emerged as a powerful paradigm for accelerating materials discovery by iteratively steering experiments toward the most promising candidates, reducing costly synthesis-and-characterization cycles. However, current AL relies predominantly on Gaussian Process (GP) and Random Forest (RF) surrogates with complementary limitations: GP underfits complex composition-property landscapes due to rigid kernel assumptions, while RF produces unreliable uncertainty estimates in small-data regimes, precisely where most materials datasets (<500 samples) reside. Here we propose In-Context Active Learning (ICAL), replacing conventional surrogates with TabPFN, a transformer-based foundation model pre-trained on millions of synthetic tasks to meta-learn a universal prior over tabular data. TabPFN performs principled Bayesian inference in a single forward pass without dataset-specific retraining, delivering well-calibrated predictive uncertainty where GP and RF fail most severely. Benchmarked against GP and RF across 10 materials datasets spanning copper alloy hardness and electrical conductivity, bulk metallic glass-forming ability, and crystal lattice thermal conductivity, TabPFN wins on 8 out of 10 datasets, achieving a mean saving of 52% in extra experiments/evaluations relative to GP and 29.77% relative to RF. Cross-validation analysis confirms that TabPFN's advantage stems from superior uncertainty calibration, achieving the lowest Negative Log-Likelihood and Area Under the Sparsification Error curve among all surrogates. This demonstrates that a pre-trained foundation model can serve as a highly effective surrogate for active learning-based materials discovery.

Keywords deep learning one-class classifier · materials discovery · graph neural network · deep learning

1 Introduction

The discovery and optimization of new materials is a central challenge in science and engineering, with far-reaching implications for energy storage, structural alloys, catalysis, semiconductors, and drug design [1, 2, 3, 4, 5, 6, 7]. Traditional Edisonian trial-and-error experimentation is both time-consuming and extraordinarily expensive. The cost of synthesizing and characterizing a single alloy or crystal material — including arc melting, X-ray diffraction, electron microscopy, and mechanical or functional property testing, with labor — ranges from approximately \$500 to \$3,000 for structural alloys and can reach \$20,000 or more for advanced functional materials. These costs create an essential bottleneck: the compositional and processing spaces of modern materials are combinatorially vast, yet only a tiny fraction can be explored experimentally. Active learning (AL), especially Bayesian Optimization (BO), has emerged as a powerful paradigm to address this challenge by coupling machine learning (ML) predictions with adaptive data acquisition, iteratively steering experiments toward the most informative or highest-performing candidates and thereby reducing the number of costly evaluations required to reach a design target [1, 8, 3, 9].

Citation*: J.Hu et al. **Foundation model based In-context active learning for accelerated materials discovery. 15 Pages.... DOI:000000/11111.

†Corresponding author: jianjunh@cse.sc.edu

The breadth of AL’s impact as a computation engine driving materials discovery is substantial and growing. In functional materials, Yuan et al. demonstrated accelerated discovery of large electrostrains in BaTiO₃-based piezoelectrics [10], and Bassman et al. applied AL to layered materials design [11]. In electrocatalysis, Moon et al. used AL to discover a champion four-metal perovskite oxide for oxygen evolution [6], Suvarna et al. streamlined development of high-performance catalysts for higher alcohol synthesis [12], and Mok et al. identified electrocatalysts for CO₂ reduction [9]. For alloy systems, Kim et al. searched for optimal multi-metallic alloy catalysts [13], and Rao et al. developed closed-loop AL frameworks for high-entropy Invar alloys [14]. Beyond metals, Kunkel et al. applied AL to organic semiconductor discovery [15]. AL has also transformed chemistry through self-driving laboratories (SDLs), which automate experimental planning and execution to accelerate the research pipeline in both chemistry and materials science [16, 17, 18, 19]. In drug design, Bayesian AL frameworks have been applied to drug screening [20] and regression-based AL has been used to accelerate large-scale virtual library docking [21]. Across all these domains, the common thread is that AL enables order-of-magnitude reductions in the number of experiments required relative to conventional design-of-experiments or random search [22, 1, 23, 24, 25].

Current Practice and Limitations of Surrogate Models in Materials Active Learning

Despite its broad success, AL in materials science is heavily dependent on the choice of surrogate model, and current practice reveals significant weaknesses in all widely used approaches. A recent comprehensive survey [3] and benchmark study [26] show that Gaussian Process (GP) regression has historically been the dominant surrogate model in Bayesian Optimization (BO)-based AL, valued for its native probabilistic output and its principled uncertainty estimates that directly enable the exploration–exploitation trade-off inherent to acquisition functions such as Expected Improvement (EI) and Upper Confidence Bound (UCB) [27, 1]. GP-based BO has been applied extensively: to catalyst design [12, 28], alloy discovery [29, 30, 31], and shape memory alloys [1], among many others. However, GP surrogates suffer from a fundamental modeling limitation: their rigid parametric assumptions about the feature–property landscape lead to high bias, making them prone to underfitting complex, nonlinear, or high-dimensional composition–property relationships [32, 3]. Furthermore, standard GPs scale cubically with data size, limiting their applicability as datasets grow [33].

Random Forest (RF) models have been proposed as a practical alternative, offering greater model flexibility, lower sensitivity to hyperparameter choice, and no strict distributional assumptions [26]. Benchmark studies confirm that RF and GP with anisotropic kernels offer comparable top-tier performance, with RF being advantageous in terms of computational cost and ease of use [26]. RF has therefore been adopted widely as a surrogate in AL for materials design too [14, 34, 35, 36]. However, RF’s high model capacity exposes it to a different failure mode: in the small-data regimes that are characteristic of experimental materials discovery [37], RF is prone to overfitting, and its uncertainty estimates — derived from ensemble variance across decision trees — are heuristic rather than principled. This makes RF uncertainty unreliable as a guide for query selection, particularly in the early iterations of an AL campaign when the training set is smallest and reliable uncertainty quantification is most critical [38].

Neural network (NN) surrogates, including multi-layer perceptrons (MLPs), deep ensembles, and graph neural networks such as ALIGNN, share RF’s high model capacity but are arguably even more susceptible to overfitting in low-data regimes due to their larger number of parameters and the absence of RF’s built-in regularization through bagging and feature subsampling [14, 38, 39]. Ensemble-based uncertainty quantification for NNs — whether through deep ensembles, Monte Carlo dropout, or bootstrapping — introduces additional computational cost and remains heuristic in nature. Deep Gaussian Processes (DGPs) have been proposed to overcome the limited expressiveness of standard GPs by stacking GP layers to model complex hierarchical feature relationships [33], while hierarchical GP frameworks have been developed to handle high-entropy alloy composition spaces [32]. Despite these advances, the fundamental dilemma remains: GP models have reliable uncertainty but insufficient modeling capacity; RF and NN models have high capacity but unreliable uncertainty in small-data regimes. This tension between model fidelity and uncertainty quality represents a core, unresolved challenge in AL-based materials discovery. In addition, the data scarcity widely exist in materials discovery. A recent survey [37] over 109 data sets, shows that ~57% have <500 samples, ~67% comprise <1000 samples and only ~21% of data sets contain >2000 samples. The small datasets inherent in materials science has posed significant challenges to machine learning and active learning [40, 41, 42]

Motivation: TabPFN as a Foundation Model Surrogate for Active Learning

To address the dual limitations of existing surrogate models, we propose using TabPFN [43]— a foundation model for tabular data — as the surrogate in a Bayesian active learning framework for materials discovery. TabPFN is a transformer-based model that has been meta-trained via in-context learning on a large corpus of synthetic tabular datasets to approximate Bayesian inference over small tabular data problems . Unlike GP, RF, and NN surrogates that are fit from scratch on each new dataset, TabPFN leverages a pre-trained prior over functions and performs inference

in a single forward pass without any gradient-based optimization on the target dataset. Critically, TabPFN outputs a full predictive distribution — not merely a point estimate with a heuristic variance proxy — because it was explicitly meta-trained to represent posterior uncertainty over tabular inputs. This makes it a principled probabilistic surrogate that is both expressive enough to capture complex composition–property relationships and capable of producing reliable uncertainty estimates in the small-data, high-dimensional settings that characterize experimental materials discovery.

We argue that these properties make TabPFN uniquely suited as a surrogate model for AL in materials science, which has demonstrated their high performance in small data materials property prediction [44]. The predominant regimes of interest — early-stage alloy design, catalyst screening, and crystal property optimization — involve datasets of tens to a few hundred labeled examples, precisely the regime where TabPFN’s meta-trained in-context inference provides the greatest advantage over both the underfitting of GP and the overfit-prone, heuristically uncertain RF and NN alternatives. Moreover, in-context learning enables TabPFN to rapidly adapt to new materials tasks without retraining, enabling seamless integration into the iterative AL loop. In this work, we propose and evaluate an In-Context Bayesian Active Learning framework that replaces conventional GP and ensemble surrogate models with TabPFN, and we additionally introduce an improved sample selection strategy that balances both quality (acquisition function score) and diversity to mitigate redundant querying — a known failure mode of greedy acquisition in materials spaces.

In this work, we propose and evaluate the In-Context Active Learning (ICAL) algorithm, which replaces conventional GP and RF surrogate models with TabPFN — a transformer-based foundation model meta-trained to approximate Bayesian inference over tabular data — for pool-based materials discovery. We benchmark ICAL against GP and RF baselines across 10 materials datasets spanning copper alloys, bulk metallic glasses, and crystal lattice thermal conductivity, covering diverse property targets and feature representations. Our main findings are as follows. First, TabPFN achieves the lowest number of extra evaluations on 8 out of 10 datasets, with a mean saving of 52% relative to GP and 29.77% relative to RF averaged across all TabPFN-winning datasets, demonstrating consistent superiority across diverse material classes and property targets. Second, TabPFN’s advantage is mechanistically grounded in superior uncertainty quantification: cross-validation experiments on the Cu-alloy electrical conductivity and LTC datasets confirm that TabPFN achieves the lowest Negative Log-Likelihood and Area Under the Sparsification Error curve among all three surrogates, confirming that its in-context posterior produces well-calibrated, informative uncertainty estimates that guide acquisition functions more efficiently than GP’s over-conservative intervals or RF’s heuristic ensemble variance. Third, we identify a critical minimum data threshold effect: TabPFN requires approximately 10–20% of the candidate pool as initial training data before its modeling advantage fully materializes, below which GP may perform comparably or better. Fourth, feature representation is a decisive factor in active learning performance that is largely independent of regression accuracy: high-dimensional Magpie features (>120 descriptors) consistently degrade AL performance for copper alloy and LTC datasets due to overfitting in the surrogate’s uncertainty estimation, while the same Magpie features yield the best AL performance for glass-forming alloy discovery where the more complex composition–property landscape benefits from richer physicochemical descriptors. Finally, we introduce normalized and hybrid acquisition functions that address the scale instability of raw acquisition scores in small-data regimes, further improving TabPFN’s active learning efficiency across datasets.

2 Method

2.1 Pool based materials discovery using active learning

Active learning-based materials design has been widely used in materials discovery [1, 45, 46]. These approaches can be broadly classified into two categories. The first is open-ended materials discovery, in which new samples are generated based on a machine learning model. The second category focuses on exploring a fixed set of candidate materials to screen for those with desired properties. While open-ended active learning design fits many realistic scenarios, it has the drawback of relying on real experimental validation or computational simulation (such as DFT) to obtain ground truth property values for evaluating algorithm performance. In contrast, using a fixed set of materials with annotated properties allows for a more direct evaluation of active learning performance. This is achieved by starting with a small proportion of samples as the initial training set and treating the remainder as unannotated. The goal is then to determine how many samples must be evaluated to find the target sample with the best property.

Our study adopts this second category of active learning-based screening for materials discovery or pool-based active learning, following the active learning materials design benchmark study in [26]. The minor difference is that our initial population is selected as a given percentage of samples with the lowest/highest properties instead of random selection to reduce the experiment uncertainty. The main framework is illustrated in Figure 1. The process begins with data ingestion and preparation, where a raw materials database is loaded, cleaned, and encoded to convert categorical features into a numerical format suitable for machine learning. The process initializes by randomly selecting a small percentage of these materials to form the initial “labeled” training set, while the remaining majority constitutes the

unlabeled pool. The core of the methodology is the iterative active learning loop. In each cycle, a surrogate AI model is trained using the current labeled data. This model is then tasked with predicting the properties of the entire unlabeled pool, outputting both a predicted mean value (μ) and an associated uncertainty (σ) for each candidate. These outputs are combined to calculate the Expected Improvement (EI), a strategic metric that balances exploration (high uncertainty) and exploitation (high predicted mean). The top- k candidates with the highest EI scores are selected for evaluation. A decision step determines if the global maximum property has been identified among these candidates. If the maximum has not been found, the selected candidates are moved from the unlabeled pool into the training set—simulating the acquisition of new experimental labels—and the model is retrained in the next iteration. Once the global maximum is successfully identified, the loop terminates, and the total number of evaluations required to find the optimal solution is reported. In AL, each surrogate model may be configured with different acquisition functions. We have evaluated six acquisition functions as different ML models may work best with different acquisition functions (Table 1).

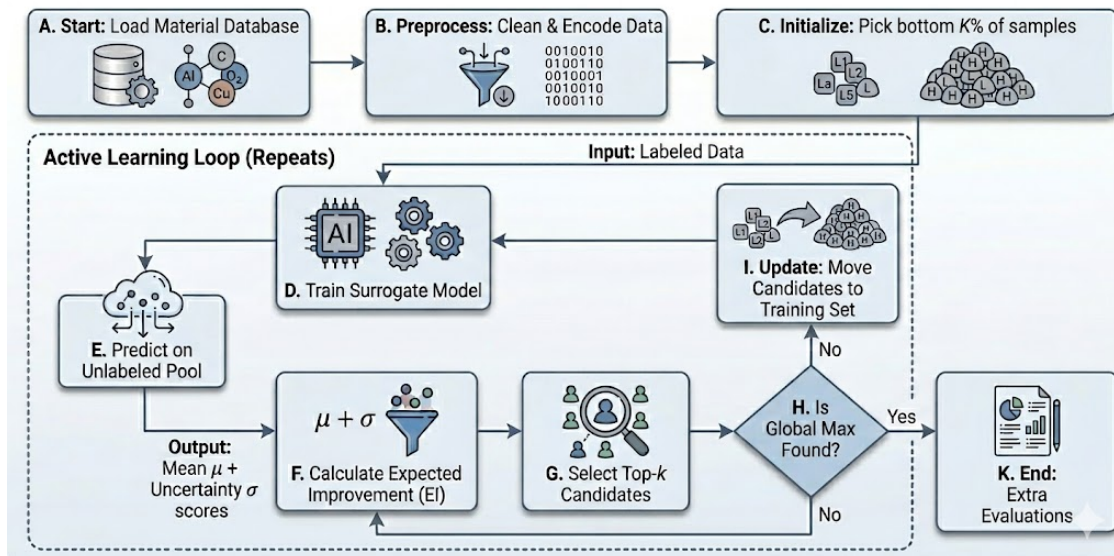


Figure 1: Pool-based active learning pipeline for discovering new materials. F: EI can be replaced with any other acquisition functions. G: $k=1$ is used for maximum sample efficiency. H: Top-1 task can be replaced with discovering Any of All of Top-K tasks.

2.2 In context active learning (ICAL) for materials discovery

Recent literature reviews find that currently the mainstream practices of active learning based materials discovery are based on Bayesian optimization with conventional machine learning surrogate models such as Gaussian Process, Random Forest, Neural networks, and gradient boosting trees [47, 26, 3, 30]. However, these surrogate models either suffer from their inherent bias and lack of complex modeling capacity or from their overfitting risk in active learning based materials discovery.

We propose the In-context Active Learning (ICAL) algorithm to address these issues in current active learning-driven materials discovery (ALMD) using TabPFN, an in-context learning foundation model, as a novel surrogate model. We benchmark it against the most widely adopted surrogate models in active learning practice, including Gaussian Processes (GP) and Random Forest (RF). Our ICAL algorithm leverages three distinctive modeling capacities of TabPFN to achieve superior active learning performance: (1) significantly stronger modeling capability for small datasets compared to GP, mitigating the underfitting risk arising from rigid parametric assumptions; (2) lower overfitting risk compared to RF (and MLP), attributed to its meta-learned inductive biases and its function regression from large-scale pretraining over synthetic regression datasets rather than relying solely on the scarce labeled data available in ALMD; and (3) native probabilistic regression capability, eliminating the need for computationally expensive ensemble methods or approximate Bayesian inference techniques such as Monte Carlo (MC) Dropout.

Normalized EI/UCB : We also recognize a fundamental issue in materials active learning. The first one is the scale issue in acquisition functions when using mean and standard deviation to calculate ranking scores, due to the extremely high variance in out-of-distribution predictions by surrogate models trained with small datasets. It is difficult to balance the mean and uncertainty. We propose to normalize both the mean and standard deviation before ranking

Table 1: Summary of Active Learning Acquisition Functions

Acquisition Strategy	Mathematical Formulation	Description & Scaling Notes
Standard UCB	$\mu(x) + \beta\sigma(x)$	Balances mean and uncertainty using raw, unnormalized values (prone to scale issues).
Normalized UCB	$\mu_{norm}(x) + \beta\sigma_{norm}(x)$	Scale-invariant. Both μ and σ are normalized to $[0, 1]$ before scaling with β .
Hybrid UCB	$\mu_{norm}(x) + \beta\sigma_{GP_norm}(x)$	Uses normalized mean from TabPFN and normalized uncertainty from a Gaussian Process.
Standard EI	$(\mu(x) - f_{best})\Phi(Z) + \sigma(x)\phi(Z)$	Calculates Expected Improvement using raw units without a trade-off parameter.
Normalized EI	$(\hat{\mu}(x) - \hat{f}_{best} - \xi)\Phi(Z) + \hat{\sigma}(x)\phi(Z)$	Calculates Expected Improvement using min-max normalized predictions and a trade-off parameter ξ , where $Z = \frac{\hat{\mu}(x) - \hat{f}_{best} - \xi}{\hat{\sigma}(x)}$.
Hybrid EI	Same as Normalized EI	Computes Normalized EI ξ utilizing the mean from TabPFN and the uncertainty from the GP.

Note: $\mu(x), \sigma(x)$: Predicted mean and standard deviation (uncertainty) for candidate material x .
 $\mu_{norm}, \sigma_{norm}$: Min-max normalized mean and standard deviation, scaled strictly to $[0, 1]$.
 β : Static exploration parameter dictating the trade-off between exploiting the mean and exploring uncertainty.
 f_{best} : The maximum target property value discovered in the dataset so far.
 ξ : A minimum threshold or trade-off parameter defining the required margin of improvement over f_{best} .
 Z : The standardized dimensionless improvement score, defined as $Z = (\mu_{norm}(x) - f_{best_norm} - \xi) / \sigma_{norm}(x)$.
 $\Phi(\cdot), \phi(\cdot)$: The Cumulative Distribution Function (CDF) and Probability Density Function (PDF) of the standard normal distribution.
 \mathcal{U}, \mathcal{N} : Uniform and Normal probability distributions.

score calculation, leading to our normalized UCB and normalized EI acquisition function (See Table 1). While this normalization may disrupt the theoretical rigor of original GP model based BO, our experiments showed that it leads to better performance for many datasets. It also brings the benefit of easy across-dataset hyper-parameter setting for e.g. the beta parameter in UCB.

Hybrid Acquisition Functions: We also propose hybrid acquisition functions (See Table 1) to exploit the high modeling capacity of TabPFN and RF and GP’s geometry-sensitive uncertainty quantification. While TabPFN demonstrates superior predictive accuracy as a surrogate model, its uncertainty quantification relies on in-context probabilistic estimates that may not fully capture the geometric structure of the feature space. Gaussian Processes, by contrast, produce uncertainty estimates grounded in kernel-based covariance functions that explicitly encode spatial correlations between data points — a property particularly valuable in materials discovery, where property landscapes often exhibit smooth, structured variation across compositional or configurational spaces. We therefore propose a hybrid acquisition function combining UCB and EI that pairs TabPFN’s mean prediction with GP’s kernel-derived variance estimation. This decoupling exploits the complementary strengths of both models: TabPFN contributes a more accurate and flexible predictive mean, especially in low-data regimes, while GP contributes geometrically informed uncertainty estimates that better reflect the local density and distribution of the labeled sample pool. The resulting hybrid acquisition strategy achieves a more effective exploration-exploitation balance, as the GP variance naturally encourages sampling in structurally underexplored regions of the feature space that TabPFN’s uncertainty estimates alone may overlook. This explains the observed performance gains on datasets whose property landscapes exhibit strong spatial correlation structure, while also clarifying why the improvement is dataset-dependent — on datasets with irregular or discontinuous property landscapes, the geometric assumptions embedded in GP’s covariance structure may offer less advantage.

To justify our ICAL active learning algorithm, we describe the characteristics of TabPFN and compare it to two baseline models GP and RF. Table 2 summarize how these models calculate their mean and uncertainty.

TabPFN: A Foundation Model Surrogate for ALMD: The Tabular Prior-Data Fitted Network (TabPFN) redefines tabular regression by framing it as a sequence-to-sequence problem, utilizing a Transformer architecture to implement In-Context Learning (ICL). Unlike traditional regressors that optimize parameters to fit a specific training set, TabPFN treats the entire dataset—consisting of feature vectors and their corresponding target values—as a sequence of input

Table 2: Summary of Predictive Mean and Uncertainty Estimation by Surrogate Models

Surrogate Model	Predictive Mean ($\mu(x)$)	Predictive Uncertainty ($\sigma(x)$)
TabPFN	The median (50th percentile) of the output distribution predicted directly by the pre-trained transformer network.	Derived from the predicted 95% confidence interval. Calculated as the difference between the 97.5th and 2.5th predicted percentiles divided by 3.92.
Random Forest (RF)	The average prediction across all T individual decision trees in the ensemble: $\mu(x) = \frac{1}{T} \sum_{t=1}^T \hat{y}_t(x)$	The standard deviation of predictions across the ensemble of trees, serving as a measure of epistemic uncertainty (model disagreement): $\sigma(x) = \sqrt{\frac{1}{T} \sum_{t=1}^T (\hat{y}_t(x) - \mu(x))^2}$
Gaussian Process (GP)	The analytical posterior predictive mean, exacted via exact probabilistic conditioning on the training data.	The analytical posterior predictive standard deviation, representing geometric uncertainty governed heavily by distance in the kernel space (e.g., RBF).

Note: For TabPFN, the 3.92 scaling factor assumes the predicted quantiles approximate a normal distribution (where $2 \times 1.96 = 3.92$ covers 95% of the density). For the Gaussian Process, both $\mu(x)$ and $\sigma(x)$ are derived analytically from the chosen covariance function.

tokens. By prepending the labeled "support set" to an unlabeled "query" sample, the Transformer’s self-attention mechanism computes the relational dependencies between the new material candidate and all previously observed experimental data points. This allows the model to perform a single forward pass that approximates the Posterior Predictive Distribution (PPD), effectively acting as a meta-learned Bayesian regressor.

TabPFN’s inherent capability for probabilistic regression allows for robust uncertainty estimation, which, when coupled with its zero-training inference, makes it an ideal candidate for Active Learning in material design; the model can instantly suggest the next optimal experimental candidate as new data points are added to the context. Compared to traditional benchmarks, TabPFN offers the predictive power of gradient-boosted trees and the rigorous uncertainty quantification of Gaussian Processes, but with significantly higher efficiency and accuracy in the low-data regimes typical of experimental materials science. This architecture is particularly potent because it replaces the rigid structure of Random Forests or the kernel-dependency of Gaussian Processes with a flexible attention-based weighting, enabling it to capture complex, non-linear interactions even in the extreme low-data regimes typical of laboratory discovery.

Baseline surrogate model: Gaussian Process: Gaussian Process (GP) has long been the standard for Active Learning (AL) based design [48, 34, 32, 49, 50] because it provides a mathematically rigorous Bayesian framework for uncertainty quantification. GP defines a prior over functions—typically assuming a specific kernel, such as the Radial Basis Function (RBF) or Matérn kernel, to encode smoothness and physical assumptions—and updates this prior into a posterior distribution as new experimental data is observed. This results in not only a mean prediction for a material’s properties but also a formally derived variance that represents the model’s confidence. In an active learning loop, this predictive variance is utilized by acquisition functions like Expected Improvement (EI) or Upper Confidence Bound (UCB) to navigate the exploration-exploitation tradeoff, systematically identifying material compositions that either maximize a target property or reduce the model’s overall ignorance. While highly effective for small datasets, GP’s reliance on manually selected kernels and its $O(n^3)$ computational complexity can limit its flexibility in capturing complex, high-dimensional chemical relationships compared to modern attention-based models like TabPFN. We also found that GP has much lower regression performance compared to Random Forest and TabPFN.

Baseline surrogate model: Random Forest Random Forest (RF) has been widely used in active learning material design [34, 38, 24, 51] due to its inherent robustness and its ability to provide heuristic uncertainty estimates through ensemble variance. In a typical AL material design loop, an RF model is trained on a sparse initial dataset of material compositions and properties; the "disagreement" or variance between the individual decision trees in the ensemble is then used as a proxy for epistemic uncertainty. This allows researchers to employ acquisition functions, such as Query-by-Committee or Upper Confidence Bound (UCB), to identify unlabeled material candidates in regions where the forest’s predictions are least consistent. While widely adopted for its resistance to overfitting and its ability to handle high-dimensional chemical descriptors with minimal tuning, RF-based active learning often faces challenges in

low-data regimes where the bootstrap samples may not provide a diverse enough "committee" for accurate uncertainty quantification—a limitation that more modern Bayesian approaches and foundation models like TabPFN aim to address.

2.3 Benchmark Datasets

We have evaluated the performance of AL algorithms based on different combination of surrogate models and acquisition functions over a set of dataset as shown in Table 3.

The first three datasets concerns lattice thermal conductivity (LTC) prediction, comprising 3,148 crystal structures. Diamond (C) was explicitly excluded from the original dataset due to its exceptionally high LTC value, which would trivialize the active learning task by making it too easily identifiable as the optimal candidate. Three datasets were constructed using three different feature representations: elemental concentration (LTC_C), Magpie features (LTC_M), and a mixed representation combining Magpie with 20 structural features (LTC_S). All features were computed using the *matminer* library [52]. The resulting feature vector for each material is a concatenation of three distinct categories: (1) *compositional features*, derived from the material’s stoichiometry and incorporating Magpie elemental property statistics, average valence orbital configurations, and ionic property approximations; (2) *structural features*, including bulk density metrics extracted directly from the crystallographic structure; and (3) *symmetry features*, encoding the space group and rotational properties of the lattice. Any missing or non-numeric values encountered during featurization were imputed to zero to ensure numerical stability in downstream modeling.

The second group of datasets are on predicting hardness and electrical conductivity of copper-based alloys [53]. The hardness dataset (Cu_HD_C/M) has 1614 samples while the electrical conductivity dataset (Cu_EC_C/M) has 1826 samples. Both come with two different feature representations including element concentrations and Magpie features.

The third group of datasets are on predicting glass-forming ability (critical casting diameter (Dmax)) of Fe-based bulk metallic glasses [54]. These are amorphous metal alloys, also known as metallic glasses that possess a unique combination of properties including very high elastic strain limit and excellent resistance to corrosion and wear, making them highly attractive for various industrial applications. The dataset has 495 samples and comes with three different representations including concentration (Glass_DS1), physical features (Glass_DS2), and Magpie features (Glass_DS3).

Table 3: Summary of 25 Benchmark Datasets

Dataset Code	Dataset	Samples	Features	Opt. Objective	
LTC_C	LTC Concentration	3,148	62	LTC	
LTC_M	LTC Magpie	3,148	126	LTC	
LTC_S	LTC Structure	3,148	146	LTC	
Cu_HD_C	Cu Alloy Hardness Concentration	1,614	34	Hardness	[53]
Cu_HD_M	Cu Alloy Hardness Magpie	1,614	132	Hardness	[53]
Cu_EC_C	Cu Alloy Elect. Conduct. Concentration	1,826	34	Electrical Conductivity	[53]
Cu_EC_M	Cu Alloy Elect. Conduct. Magpie	1,826	132	Electrical Conductivity	[53]
Glass_DS1	Bulk glass forming alloy Concentration	495	22	glass forming	[54]
Glass_DS2	Bulk glass forming alloy Physical	495	14	glass forming	[54]
Glass_DS3	Bulk glass forming alloy Magpie	495	145	glass forming	[54]

3 Results

3.1 Performance evaluation of ICAL in active-learning based materials discovery

We evaluate the performance of AL algorithms with three surrogate functions (GP, RF, TabPFN) combined with the six acquisition functions. For a given dataset, the pool-based materials discovery process starts with a given percentage of initial population of samples with the lowest property values and use the active learning cycles to locate the global optimum with batch size of 1. The extra evaluation steps during the AL cycles are used as the performance metric. For each surrogate model, we pick its best acquisition function based on the mean extra evaluations needed to locate the global optimum averaged across all 19 init levels (5%–95%). For GP and RF, we repeat the experiments for 20 times to count their randomness while TabPFN has no such randomness. We have tuned the hyper-parameters for the UCB and normalized UCB and normalized EI acquisition functions. We set the β to 30 and ξ to 0.2 across all experiments and all datasets for simplicity.

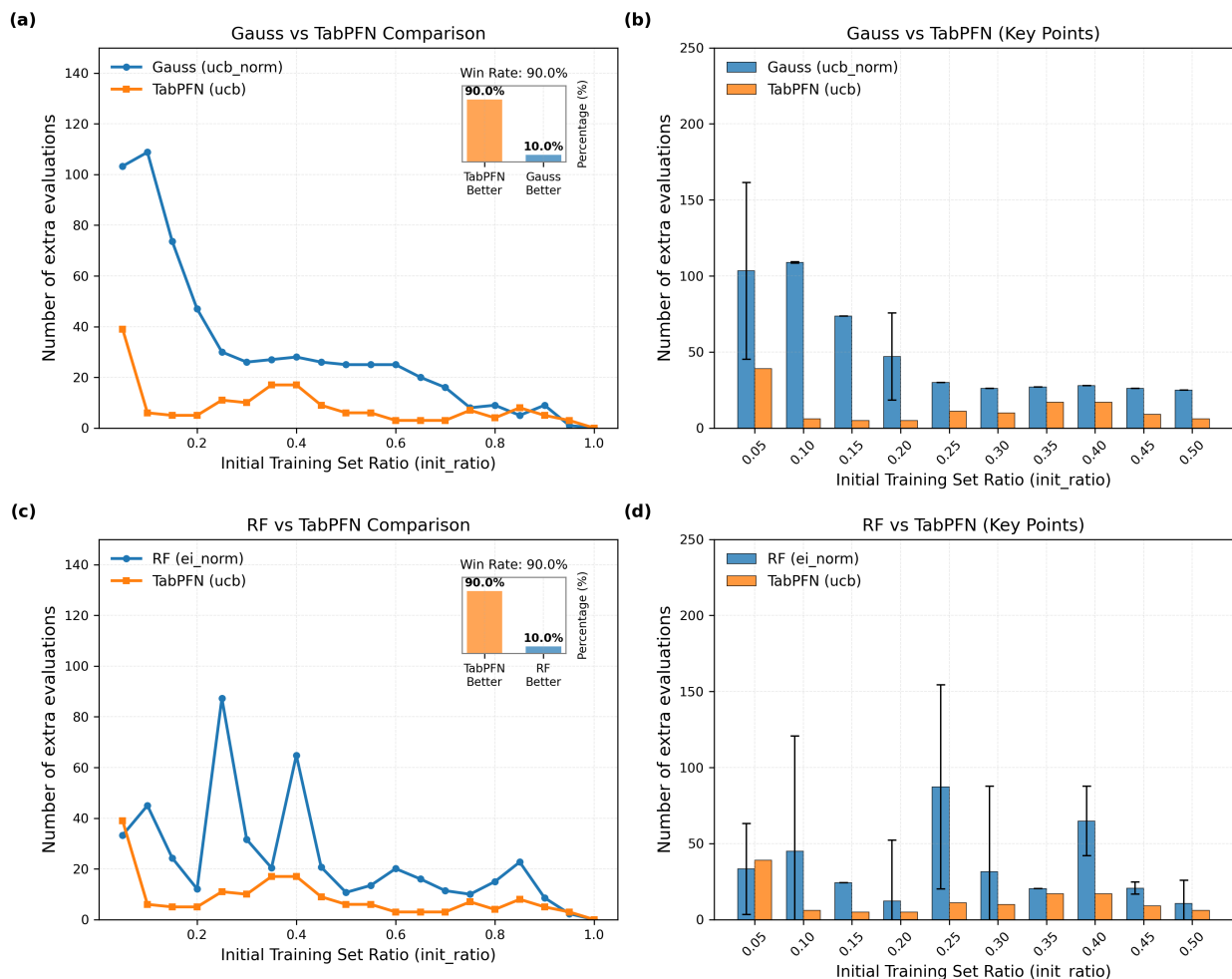
Dataset: cu_hardness


Figure 2: Performance of ICAL on *Cu_hardness* dataset compared to GP and RF based AL. (a-b) TabPFN against GP; (c-d): TabPFN against RF.

Figure 2 presents the active learning performance on the *cu_hardness* dataset, where the target property is copper alloy hardness and the metric is the number of extra evaluations required to identify the global optimum beyond the initial training set (lower is better). TabPFN with UCB acquisition achieves a 90% win rate against both GP (UCB-norm) and RF (EI-norm) baselines — the highest win rate observed across all datasets tested — demonstrating a remarkably consistent and large performance advantage. As shown in panels (a) and (b), GP requires up to ~110 extra evaluations at low *init_ratio* (0.05–0.10), while TabPFN reduces this to ~38 and ~5 respectively, representing a 3–20 \times reduction in experimental effort in the most data-scarce regime. This advantage persists monotonically as *init_ratio* increases, with TabPFN consistently requiring fewer than 20 extra evaluations across all conditions beyond *init_ratio* = 0.15, while GP remains elevated at 25–50 evaluations through mid-range *init_ratio*s. The RF comparison (panels c and d) reveals an even more problematic failure mode: RF (EI-norm) exhibits severe instability, with multiple sharp spikes reaching ~85 extra evaluations at *init_ratio* \approx 0.25 and ~65 at *init_ratio* \approx 0.40. These spikes directly reflect RF’s well-known weakness in small-data regimes, where its heuristic ensemble variance produces unreliable uncertainty estimates that mislead the EI acquisition function into querying uninformative or redundant compositions. Critically, panel (d) shows that RF’s error bars are extraordinarily large — extending to ~155 at *init_ratio* = 0.25 — meaning that in a single experimental campaign, a practitioner using RF could require over 150 additional synthesis-and-characterization cycles to find the optimal hardness alloy, at a potential cost exceeding \$300,000 at conservative per-sample estimates. In stark contrast, TabPFN maintains both low mean extra evaluations and tight error bars throughout, confirming

that its meta-trained in-context posterior provides not only superior average efficiency but also reliable, reproducible convergence that is essential for practical materials discovery workflows.

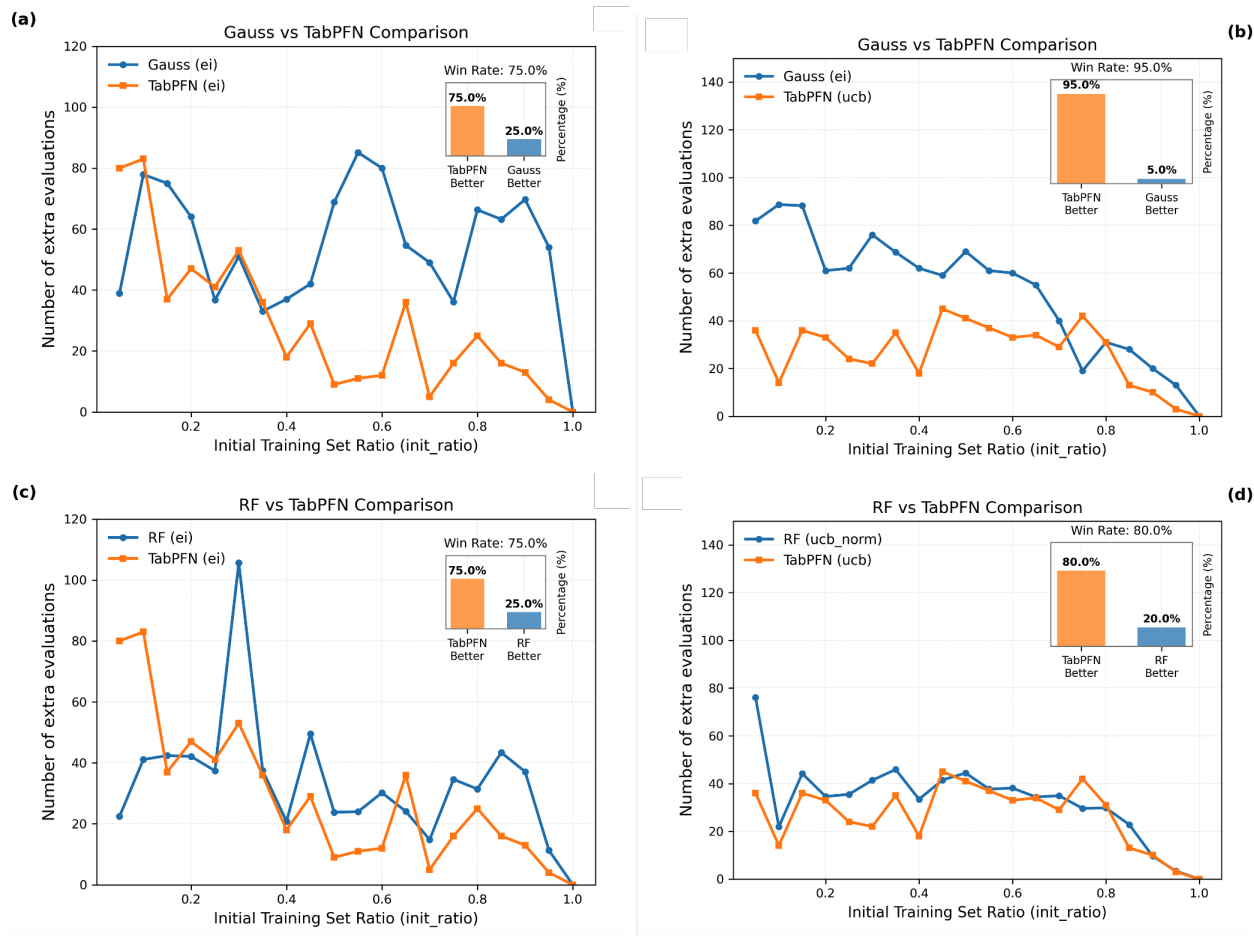


Figure 3: Performance of ICAL on (a) (c) Cu_electric dataset and (b) (d) Glass_DS3 dataset compared to GP and RF based AL.

Figure 3 (a) shows the active learning results on the *cu_electric* dataset targeting electrical conductivity, where TabPFN (EI) achieves a **75% win rate** against both GP (EI) and RF (EI) baselines. Unlike the *cu_hardness* dataset where TabPFN’s advantage was consistent across all *init_ratios*, a notable exception emerges here at very low initial training set sizes (*init_ratio* ≤ 0.15): TabPFN requires ~ 80 – 83 extra evaluations, slightly *exceeding* GP’s ~ 38 – 79 and RF’s ~ 22 – 42 in this regime. This reversal suggests that TabPFN’s in-context posterior requires a minimum amount of task-specific data to form a reliable representation of the conductivity landscape before its modeling advantage over GP and RF materializes. Beyond *init_ratio* ~ 0.20 , however, TabPFN’s superiority becomes pronounced and sustained: GP remains persistently elevated at 40–85 extra evaluations with a notable peak at *init_ratio* ≈ 0.55 (~ 85), while TabPFN drops to below 15 evaluations across the same range. RF (panel c) exhibits its characteristic erratic behavior with a sharp spike to ~ 105 at *init_ratio* ~ 0.30 , further confirming the unreliability of ensemble-variance-based uncertainty quantification in sparse data regimes. Both curves converge toward zero at *init_ratio* $\rightarrow 1.0$, as expected when the training set covers nearly the entire candidate space. The crossover behavior at low *init_ratios* is an important practical finding: it suggests that a minimum initial dataset size — approximately 15–20% of the candidate pool — should be collected before deploying TabPFN-based active learning for electrical conductivity optimization.

Figure 3 (b) (d) presents results on the *glass_DS3* dataset with magpie features targeting glass forming capability of alloys. TabPFN (UCB) achieves its highest win rate across all datasets tested: **95%** against GP (EI) and **80%** against RF (UCB-norm), suggesting that the glass forming capability landscape is particularly well-suited to TabPFN’s in-context Bayesian inference. Identifying glass-forming alloys is notoriously challenging due to the complex, nonlinear interplay between compositional features and the tendency to avoid crystallization — precisely the kind of structure that GP’s

rigid kernel assumptions fail to capture. As shown in the upper panel, GP requires 60–90 extra evaluations across nearly the entire `init_ratio` range of 0.05–0.65, while TabPFN stays consistently below 45 throughout, representing a **2–4× reduction** in the number of alloy synthesis and characterization experiments needed. This is practically significant given that producing and validating a glass-forming alloy — involving arc melting, melt spinning, and structural characterization via XRD to confirm amorphous phase formation — is among the more expensive experimental workflows in alloy design. The RF comparison (lower panel) tells a more nuanced story: RF and TabPFN perform comparably in the mid-range (`init_ratio` = 0.45–0.75), with curves frequently crossing, which accounts for RF’s 20% win rate — the highest any baseline achieves across all datasets. Nevertheless, TabPFN maintains a decisive advantage at low `init_ratios` where it matters most, with RF spiking to ~77 extra evaluations at `init_ratio` = 0.05 while TabPFN requires only ~37, and TabPFN’s overall smoother trajectory confirming more reliable convergence toward the optimal glass-forming composition.

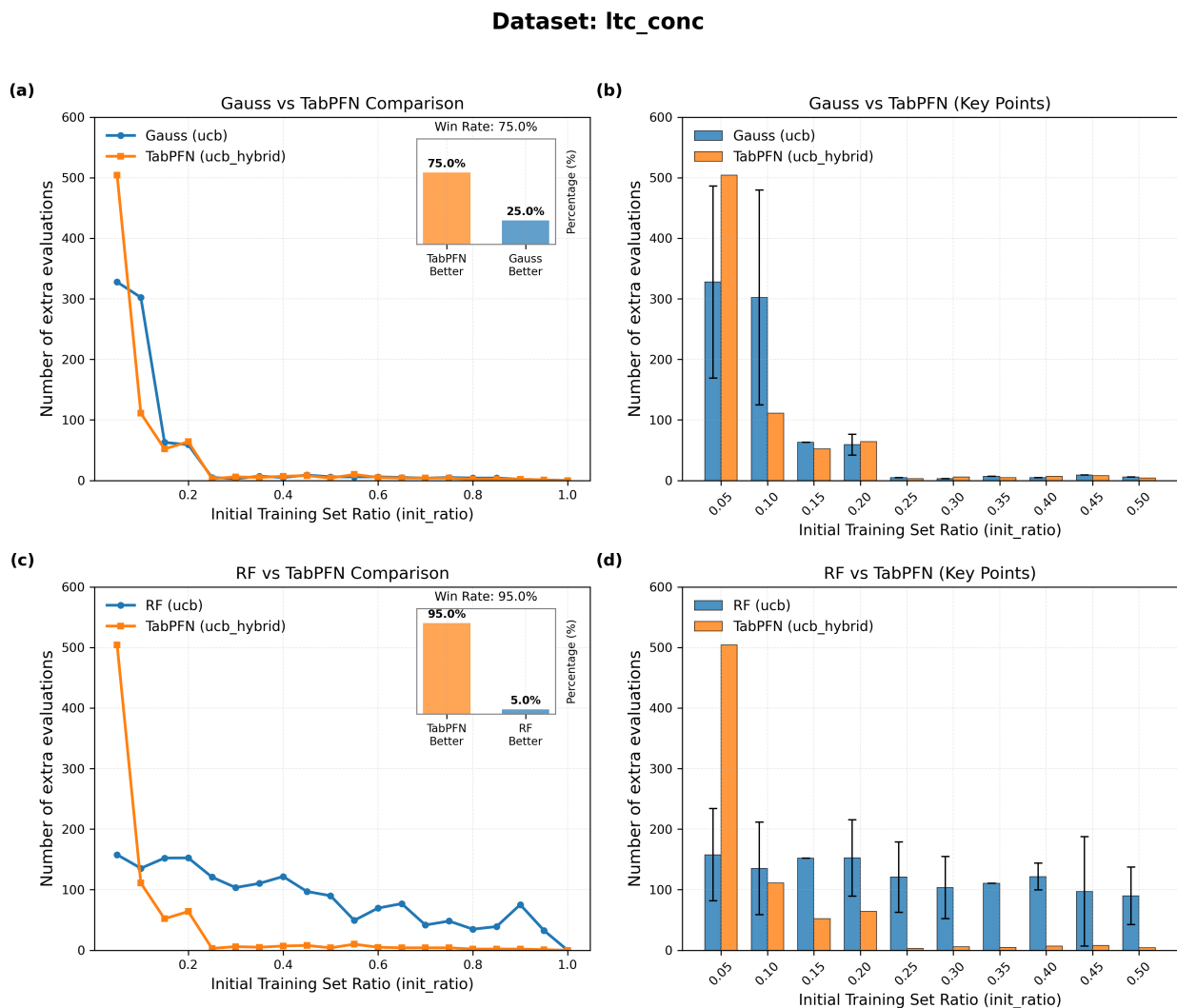


Figure 4: Performance of ICAL on LTC_conc dataset with element concentration features compared to GP and RF based AL.

Figure 4 presents active learning results on the *ltc_conc* dataset targeting the lattice thermal conductivity (LTC) of crystal materials described by concentration features. Several distinctive and noteworthy patterns emerge that set this dataset apart from the others. TabPFN (UCB_hybrid) achieves a 75% win rate against GP (UCB) and a remarkable 95% win rate against RF (UCB) — the highest RF win rate across all datasets tested — indicating that RF is particularly ill-suited for navigating the LTC–composition landscape of crystal materials when only concentration features are used. The most striking observation in this dataset is the dramatic collapse to fewer than 10 extra evaluations beyond `init_ratio` \approx 0.20: both GP and TabPFN achieve this near-perfect convergence all the way to `init_ratio` = 1.0 (panels a

and b). This suggests that the LTC landscape of crystal materials parameterized by concentration features is relatively low-complexity and well-structured — once roughly 20% of the compositional space is sampled, the global optimum becomes straightforward to locate for both GP and TabPFN surrogates. This is physically intuitive: LTC in crystals is governed primarily by phonon scattering mechanisms, which are strongly correlated with atomic mass contrast and bond stiffness — both of which vary smoothly with elemental concentration — producing a relatively smooth and navigable property landscape compared to mechanical properties or glass-forming ability. However, this result is still surprising as accurate prediction of LTC is extremely difficult by itself, showing the different ML model capability required for AL.

However, the critical distinction between TabPFN and GP lies in the extremely data-scarce regime ($\text{init_ratio} = 0.05\text{--}0.10$), where the difference is both large and practically consequential. At $\text{init_ratio} = 0.05$, GP requires ~ 330 extra evaluations while TabPFN requires ~ 500 — a rare case where TabPFN is *worse* at the smallest init size, consistent with the minimum data threshold effect observed in the `cu_electric` dataset. At $\text{init_ratio} = 0.10$, however, the roles reverse sharply: GP still needs ~ 305 extra evaluations while TabPFN drops precipitously to ~ 110 , a nearly $3\times$ reduction. This crossover between $\text{init_ratio} = 0.05$ and 0.10 defines a critical threshold: below it, TabPFN lacks sufficient in-context examples to infer the LTC–composition mapping of the crystal system; above it, its superior modeling capacity enables rapid identification of the optimum.

The RF comparison (panels c and d) is even more revealing. RF (UCB) fails catastrophically and persistently: it requires 100–160 extra evaluations across the entire range from $\text{init_ratio} = 0.15$ to 0.50 (panel d), never converging to fewer than 10 extra evaluations even when 50% of the candidate crystal compositions have been labeled. This is a qualitatively different failure mode from GP — RF does not merely need more data to converge, it fails to converge efficiently at all in this crystal composition feature space. The large error bars on RF in panel (d) further confirm that RF’s UCB-guided search is highly sensitive to random seed, producing wildly inconsistent outcomes across runs — a serious liability when synthesizing and characterizing crystal materials carries significant cost and effort. TabPFN, by contrast, converges to fewer than 10 extra evaluations by $\text{init_ratio} = 0.25$ with tight variance, demonstrating that the UCB_hybrid acquisition combined with TabPFN’s calibrated uncertainty is both efficient and reproducible for crystal LTC optimization.

Importance of representation Due to the extremely small datasets in typical materials AL, we find that the AL performance strongly depends on the features used in surrogate models. To investigate this issue, we test different features for the four datasets `cu_electric`, `cu_hardness`, `glass forming alloy`, and `LTC`. We calculate the mean number of extra evaluations per surrogate model with its best acquisition function.

Table 4: Mean number of extra evaluations per surrogate model averaged across all 19 `init_ratio` levels (5%–95%), using each model’s best acquisition function for that dataset. Percentage of extra evaluation saving achieved by TabPFN relative to GP and RF are shown in the final two columns; negative values indicate TabPFN underperforms the baseline (only for the inappropriate `magpie` feature sets).

Dataset	Gauss GP	RF	TabPFN	Winner	Best Acq (TabPFN)	% Saving. (vs GP)	% Saving. (vs RF)
<code>cu_electric</code>	58.5	37.5	[30.1]	TabPFN	<code>ei</code>	48.5%	19.7%
<code>cu_electric_magpie</code>	82.5	90.3	83.9	Gauss	<code>ucb_norm</code>	−1.7%	7.1%
<code>cu_hardness</code>	31.3	18.8	[8.8]	TabPFN	<code>ucb</code>	71.9%	53.2%
<code>cu_hardness_magpie</code>	21.9	23.5	24.1	Gauss	<code>ei_hybrid</code>	−10.0%	−2.6%
<code>glass_ds1_conc</code>	72.4	66.0	48.8	TabPFN	<code>ucb_norm</code>	32.6%	26.1%
<code>glass_ds2_physical</code>	37.6	43.7	32.6	TabPFN	<code>ucb_norm</code>	13.3%	25.4%
<code>glass_ds3_magpie</code>	67.5	31.6	[28.2]	TabPFN	<code>ucb</code>	58.2%	10.8%
<code>ltc_conc</code>	56.55	61.8	[39.9]	TabPFN	<code>ucb_hybrid</code>	29.4%	35.4%
<code>ltc_magpie</code>	243.88	44.17	41.70	TabPFN	<code>ucb</code>	82.9%	5.6%
<code>ltc_structure</code>	237.37	55.05	84.1	RF	<code>ei</code>	−64.6%	−52.8%
Mean saving of Extra Evaluations by TabPFN						52%	29.77%

Table 4 summarizes the mean number of extra evaluations per model averaged across all 19 `init_ratio` levels (5%–95%), using each model’s best acquisition function per dataset. TabPFN achieves the lowest extra evaluations on 8 out of 10 datasets, establishing it as the consistently dominant surrogate across diverse material classes and property targets.

Averaged across all TabPFN-winning datasets, TabPFN reduces extra evaluations by 35–83% relative to GP and 10–53% relative to RF, representing substantial savings in experimental cost.

A particularly important finding emerges when comparing concentration-based versus Magpie feature sets for the copper and LTC datasets. For `cu_electric`, TabPFN with concentration features requires only 30.1 extra evaluations on average, compared to 58.5 (GP) and 37.5 (RF) — reductions of 49% and 20% respectively. However, switching to the high-dimensional Magpie feature set (`cu_magpie_electric`, >120 features) reverses the winner entirely: GP becomes best at 82.5 extra evaluations, while TabPFN degrades to 83.9 — nearly indistinguishable from GP and worse than both concentration-feature models. A similar pattern holds for `cu_hardness`: TabPFN achieves only 8.8 extra evaluations with concentration features (reductions of 72% vs. GP and 53% vs. RF), but with Magpie features (`cu_magpie_hardness`) GP wins at 21.9, and all three models perform substantially worse than their concentration-feature counterparts. The same trend is observed for LTC crystal materials: `ltc_conc` gives TabPFN a win at 39.9 extra evaluations (reductions of 29% vs. GP and 35% vs. RF), whereas `ltc_magpie` produces a dramatically inflated GP count of 243.88 — a 6× degradation relative to `ltc_conc` — before TabPFN partially recovers to 41.70. These results consistently indicate that high-dimensional Magpie features introduce severe overfitting in GP’s kernel estimation and destabilize RF’s ensemble variance, undermining the uncertainty quantification that drives acquisition function decisions. TabPFN is more robust to this feature dimensionality increase, but still performs best with the leaner concentration feature representation. This additionally shows that the AL needs different model capability than the regular regression performance to achieve high performance: the magpie feature can obtain better LTC prediction models, but not necessarily better AL performance.

In contrast, the glass-forming alloy datasets reveal a strikingly different trend with respect to feature complexity. All three glass datasets are won by TabPFN, with mean extra evaluations of 48.8 (`glass_ds1`, concentration features), 32.6 (`glass_ds2`, physical features), and 28.2 (`glass_ds3`, Magpie features) respectively. Notably, performance *improves* monotonically as feature richness increases — the opposite of what is observed for copper and LTC datasets. The Magpie feature set yields the best result for glass-forming ability prediction, reducing extra evaluations by 58% relative to GP (67.5) and 11% relative to RF (31.6). This suggests that glass-forming ability is governed by a more complex, nonlinear composition–property relationship that genuinely benefits from richer physicochemical descriptors: predicting whether an alloy will form an amorphous phase depends on subtle electronic structure, atomic size mismatch, and thermodynamic factors that concentration features alone cannot adequately encode, but which Magpie descriptors partially capture. This stands in direct contrast to copper hardness and LTC, where the property landscape is smoother and high-dimensional Magpie features introduce more noise than signal. The feature-set sensitivity thus appears to be material-class dependent, and the consistent superiority of TabPFN across all three glass datasets — regardless of feature type — further demonstrates its robustness to feature space variations. Finally, `ltc_structure` is the only dataset where RF wins (84.1 extra evaluations for TabPFN vs. 55.05 for RF), suggesting that structural features present a unique inductive bias that RF’s decision-tree architecture exploits more effectively than TabPFN’s tabular meta-prior in this specific setting.

We also calculate the percentages of saving by using TabPFN based AL. Across the 10 datasets evaluated, TabPFN achieves a mean saving of 52% in extra evaluations relative to GP and 29.77% relative to RF when averaged over the datasets where TabPFN wins with the best-performing feature set, demonstrating its consistent superiority as a surrogate model for active learning-based materials discovery.

For the copper alloy datasets, the choice of feature set critically determines performance. With concentration features, TabPFN reduces extra evaluations by 48.5% vs. GP and 19.7% vs. RF for electrical conductivity (`cu_electric`), and by an even larger margin of 71.9% vs. GP and 53.2% vs. RF for hardness (`cu_hardness`) — the largest reduction against RF across all datasets. These results confirm that concentration features provide the best-performing representation for copper alloy properties, and the corresponding Magpie feature variants (`cu_electric_magpie`, `cu_hardness_magpie`) are excluded from the mean saving calculation as they do not represent the optimal feature set for most surrogate models on these material systems.

For the glass-forming alloy datasets, TabPFN wins across all three feature representations, but performance improves monotonically with feature richness. The Magpie feature set (`glass_ds3_magpie`) yields the best TabPFN result with 28.2 extra evaluations, achieving savings of 58.2% vs. GP and 10.8% vs. RF, and is therefore selected as the best-performing feature set for this material class. The physical feature set (`glass_ds2_physical`) offers a balanced alternative with savings of 13.3% vs. GP and 25.4% vs. RF, while the concentration feature set (`glass_ds1_conc`) provides the most modest gains at 32.6% vs. GP and 26.1% vs. RF. The progressive improvement from concentration to physical to Magpie features suggests that glass-forming ability is governed by complex physicochemical interactions that benefit from richer descriptors, in contrast to copper alloy properties.

For the lattice thermal conductivity (LTC) datasets, TabPFN with concentration features (`ltc_conc`) achieves savings of 29.4% vs. GP and 35.4% vs. RF and is selected as the best-performing feature set for the mean saving calculation, as the Magpie variant (`ltc_magpie`) offers only marginal additional improvement over RF (5.6%) despite a dramatic

82.9% reduction vs. GP — the latter being inflated by GP’s catastrophic failure with high-dimensional Magpie features rather than a genuine improvement in the active learning loop. The ltc_structure dataset is the sole case where TabPFN underperforms, with RF winning at 55.05 extra evaluations vs. TabPFN’s 84.1, suggesting that structural features encode an inductive bias that RF’s decision-tree architecture exploits more effectively than TabPFN’s tabular meta-prior; this dataset is excluded from the mean saving calculation accordingly. Taken together, the feature set analysis reveals a consistent principle: TabPFN performs best with the leanest feature representation that adequately captures the relevant physics of the target property, while high-dimensional feature sets only benefit TabPFN when the property landscape is sufficiently complex to warrant richer descriptors, as in the case of glass-forming ability.

3.2 Mechanism Analysis: Explaining TabPFN’s active-learning performance

The efficiency of an active learning framework is fundamentally limited by the surrogate model’s ability to balance exploitation (via accurate mean prediction) and exploration (via calibrated uncertainty estimates). To evaluate the underlying mechanisms driving the active learning performance, we conducted a comprehensive assessment of the regression accuracy and uncertainty quantification (UQ) capabilities of the three surrogate models (TabPFN, RF, and GP) over the Cu-alloy electric conductivity dataset, as summarized in Table 5. All results are based on 5-fold cross-validation. Beyond standard error metrics like RMSE and R^2 , we specifically prioritized the Spearman Rank Correlation (ρ) and Negative Log-Likelihood (NLL). In the context of materials screening, the Spearman metric is particularly critical because active learning acquisition functions (e.g., Expected Improvement) rely on the *relative ranking* of candidates to prioritize the next set of experiments, rather than their absolute predicted values.

Table 5: Uncertainty Quantification & Regression Performance Comparison. Values are reported as Mean \pm Standard Deviation. Arrows indicate whether lower (\downarrow) or higher (\uparrow) values are better. All are 5-Fold Cross-Validation Results for Cu-alloy Electrical Conductivity dataset (%IACS). Best results are highlighted in **bold**.

Model	RMSE \downarrow	R^2 \uparrow	Spearman \uparrow	NLL \downarrow	PICP (0.95)	MPIW \downarrow	AUSE \downarrow
Gaussian Process	8.38 \pm 0.51	0.73 \pm 0.04	0.81 \pm 0.02	3.46 \pm 0.03	0.93 \pm 0.01	32.50 \pm 1.02	5.58 \pm 0.16
Random Forest	5.86 \pm 0.28	0.87 \pm 0.02	0.89 \pm 0.02	3.11 \pm 0.25	0.87 \pm 0.02	15.93 \pm 0.35	1.77 \pm 0.42
TabPFN	5.56 \pm 0.42	0.88 \pm 0.03	0.92 \pm 0.01	2.34 \pm 0.15	0.88 \pm 0.02	11.16 \pm 0.34	0.83 \pm 0.12

As shown in the Table 5, TabPFN achieves a dominant regression performance with the lowest RMSE (5.56) and the highest Spearman correlation (0.92), significantly outperforming the Gaussian Process ($\rho = 0.81$). This indicates that TabPFN serves as a superior “exploitation” engine, ensuring that the candidates identified as high-value are statistically more likely to be true positives compared to the baselines.

In terms of uncertainty quantification—which governs the “exploration” efficiency of the active learning loop—we utilized the NLL, Prediction Interval Coverage Probability (PICP), Mean Prediction Interval Width (MPIW), and the Area Under the Sparsification Error (AUSE) curve. PICP measures the probability that the true value falls within the predicted confidence interval (target 0.95), while MPIW measures the sharpness of those intervals. A useful uncertainty estimate must balance high coverage with narrow width. First we found that TabPFN achieved the lowest NLL (2.34) compared to the Gaussian Process (3.46) and Random Forest (3.11), a result that is significant because NLL is a proper scoring rule that penalizes both prediction error and poor uncertainty calibration; this confirms that TabPFN’s predicted posterior distributions are the most faithful to the true data distribution. Next, while the Gaussian Process achieved high coverage (PICP \approx 0.93), it did so by producing excessively wide intervals (MPIW \approx 32.50), rendering the uncertainty signal uninformative for distinguishing between candidates. In contrast, TabPFN achieved comparable coverage with 3x sharper intervals (MPIW \approx 11.16) and the lowest AUSE (0.83) compared to 15.58 of GP and 1.77 of RF. The low AUSE score is particularly telling, as it quantifies the correlation between estimated uncertainty and actual prediction error; a low score implies that the model is “honestly” uncertain only when it is likely to be wrong. This superior calibration allows the TabPFN-driven acquisition function to efficiently navigate the chemical space, avoiding the “blind” exploration often caused by the over-conservative uncertainty estimates of standard Gaussian Processes.

We also evaluated the performances of TabPFN and the baseline ML models over the more challenging material design for higher LTC using the concentration features as shown in Table 6, which presents five-fold cross-validation results evaluating both predictive accuracy and uncertainty quantification quality for the three surrogate models on the LTC dataset with concentration features. While all three models achieve comparable predictive accuracy — TabPFN and RF both attain RMSE \approx 48.7 and $R^2 = 0.18$, modestly outperforming GP whose R^2 of -0.01 indicates near-zero predictive power — the critical differentiator lies in the quality of uncertainty estimation, which directly governs active learning query selection. GP’s near-perfect PICP of 0.99 is deceptive: it is achieved trivially through extremely wide prediction intervals (MPIW = 237.23, nearly $10\times$ larger than TabPFN’s 33.16), meaning GP’s uncertainty covers almost the entire output range regardless of input and provides no meaningful signal for distinguishing informative from uninformative

candidates. This pathological overestimation of uncertainty explains GP’s poor active learning performance on ltc_conc in Table 4, where it requires 56.55 extra evaluations on average — 29.4% more than TabPFN. RF achieves a tighter MPIW of 24.37 but significantly undercovers at PICP = 0.86, falling well short of the nominal 95% level and indicating that its heuristic ensemble variance systematically underestimates true predictive uncertainty, which in turn causes the acquisition function to over-exploit overconfident predictions and miss the global optimum — consistent with RF requiring 61.8 extra evaluations in Table 4. TabPFN achieves the best balance: a PICP of 0.94 closest to the nominal 95% coverage, a well-controlled MPIW of 33.16, the lowest NLL of 3.22 (less than half of GP’s 5.81 and less than half of RF’s 7.53), and the lowest AUSE of 2.16 — less than half of RF’s 4.50 and five times lower than GP’s 10.80. The AUSE metric is particularly relevant here as it directly measures how well-ordered the uncertainty estimates are for active learning: a low AUSE means that samples flagged as uncertain by the surrogate are indeed the ones with the largest prediction errors, enabling the acquisition function to query the most informative compositions efficiently. This superior uncertainty calibration is the mechanistic explanation for TabPFN’s 29.4% and 35.4% savings in extra evaluations relative to GP and RF respectively on ltc_conc in Table 4, and underscores that predictive accuracy alone is insufficient to characterize surrogate quality for active learning — reliable and calibrated uncertainty quantification is equally, if not more, important.

Table 6: Five-fold cross-validation results on the LTC dataset with concentration features. Values are reported as mean \pm standard deviation across folds. Arrows indicate whether lower (\downarrow) or higher (\uparrow) values are better. PICP: prediction interval coverage probability; MPIW: mean prediction interval width; AUSE: area under the sparsification error curve. Best results are highlighted in bold.

Model	RMSE \downarrow	R ² \uparrow	Spearman \uparrow	NLL \downarrow	PICP (95%)	MPIW \downarrow	AUSE \downarrow
Gaussian Process	53.26 \pm 33.75	-0.01 \pm 0.01	0.61 \pm 0.04	5.81 \pm 1.08	0.99 \pm 0.00	237.23 \pm 39.87	10.80 \pm 3.56
Random Forest	48.62 \pm 32.22	0.18 \pm 0.06	0.83 \pm 0.01	7.53 \pm 3.42	0.86 \pm 0.02	24.37 \pm 2.74	4.50 \pm 1.84
TabPFN	48.86 \pm 32.78	0.18 \pm 0.06	0.86 \pm 0.01	3.22 \pm 0.32	0.94 \pm 0.01	33.16 \pm 3.47	2.16 \pm 0.43

4 Discussion and Conclusion

In this work, we proposed and evaluated the In-Context Active Learning (ICAL) algorithm, which leverages TabPFN — a transformer-based foundation model pre-trained to approximate Bayesian inference over tabular data — as a principled surrogate for pool-based active learning in materials discovery. Benchmarked across 10 datasets spanning copper alloys, bulk metallic glasses, and crystal lattice thermal conductivity, ICAL achieves a mean saving of 52% in extra evaluations relative to GP and 29.77% relative to RF, winning on 8 out of 10 datasets. These results establish TabPFN as a consistently superior surrogate that resolves the fundamental tension between modeling capacity and uncertainty reliability that has constrained GP and RF-based active learning in materials science.

Our mechanistic analysis reveals that TabPFN’s active learning advantage is not merely a consequence of better regression accuracy — indeed, TabPFN and RF achieve comparable RMSE and R² on several datasets — but rather stems from its superior uncertainty quantification. By meta-learning a universal prior over tabular regression tasks from millions of synthetic datasets, TabPFN produces well-calibrated predictive posteriors that GP and RF, both trained from scratch on scarce experimental data, cannot replicate. This is particularly consequential in the early iterations of an AL campaign, where the training set is smallest and the quality of uncertainty estimates most directly determines whether the acquisition function explores productively or wastes evaluations on uninformative candidates. The consistently lower NLL and AUSE scores achieved by TabPFN across both the Cu-alloy and LTC datasets confirm that its in-context posterior faithfully represents predictive uncertainty in precisely these critical low-data regimes.

Several important practical insights emerge from our experiments. First, feature representation is a decisive and often underappreciated factor in AL performance, independent of regression accuracy: high-dimensional Magpie features degrade AL performance for copper alloys and LTC despite improving standalone regression metrics, while the same features benefit glass-forming alloy discovery where the property landscape is more complex. This finding suggests that feature selection for AL should be guided by AL performance metrics rather than cross-validation accuracy alone. Second, a minimum initial dataset size of approximately 10–20% of the candidate pool is required before TabPFN’s in-context advantage fully materializes, below which insufficient context examples limit its ability to infer the composition–property mapping. Practitioners should account for this threshold when designing AL campaigns with very small initial budgets. Third, our proposed normalized and hybrid acquisition functions effectively address the scale instability that plagues standard EI and UCB in small-data regimes, and are broadly applicable regardless of surrogate model choice.

The broader implications of ICAL extend well beyond the alloy and crystal datasets evaluated here. TabPFN’s pre-trained small-data regression and uncertainty quantification capabilities make ICAL a natural fit for any AL application where labeled data is expensive to acquire and datasets are small. In molecule discovery and drug design, where the cost of synthesizing and assaying candidate compounds is high and datasets are routinely small [55, 21, 20], ICAL could accelerate the identification of lead compounds by reducing the number of wet-lab evaluations required to locate optimal candidates. The regression-based active learning framework we adopt is directly analogous to virtual screening workflows used in ultra-large library docking [21], and TabPFN’s single-pass inference makes it computationally practical even when acquisition decisions must be made rapidly across millions of candidates. In catalyst design, where active learning has already demonstrated order-of-magnitude reductions in experimental effort [12, 6, 56], ICAL’s improved uncertainty calibration could further sharpen the exploration–exploitation balance and reduce the number of costly electrochemical characterization experiments.

ICAL is also well-positioned for integration into self-driving laboratory (SDL) platforms [16, 17, 18, 19], where the surrogate model must make reliable query decisions in real time with continuously growing but always small labeled datasets. TabPFN’s zero-retraining inference — performing a complete Bayesian update in a single forward pass as new experimental results are added to the context — aligns naturally with the closed-loop, iterative experimentation paradigm of SDLs, eliminating the retraining latency that can become a bottleneck in high-throughput autonomous workflows. Furthermore, ICAL can be straightforwardly extended from pool-based screening to open-ended generative materials design [3, 2], where candidate materials are proposed by a generative model and TabPFN serves as the screening surrogate to prioritize which generated candidates are worth evaluating experimentally.

Several limitations of the current work point toward promising directions for future research. The performance reversal on the *ltc_structure* dataset, where RF outperforms TabPFN, suggests that structural features encode an inductive bias that TabPFN’s tabular meta-prior does not currently capture. Extending TabPFN’s pre-training distribution to include structure-aware representations, or developing hybrid architectures that combine TabPFN’s probabilistic inference with graph neural network encoders for structural features, could address this limitation. The identified minimum data threshold effect also motivates the development of adaptive initialization strategies that ensure sufficient compositional coverage before the AL loop begins. Finally, while we evaluate single-objective AL in this work, extending ICAL to multi-objective settings [28] — where practitioners simultaneously optimize multiple competing properties such as strength and ductility, or conductivity and corrosion resistance — represents a natural and practically important extension that we leave for future work.

In conclusion, ICAL establishes TabPFN-based in-context Bayesian active learning as a principled, practical, and broadly applicable framework for data-efficient materials discovery. By resolving the long-standing tension between modeling capacity and uncertainty reliability in small-data surrogate modeling, ICAL reduces the number of expensive experiments needed to find optimal materials by up to 72% relative to GP and 53% relative to RF on individual datasets, with mean savings of 52% and 29.77% respectively across all benchmarks. Given the \$500–\$20,000 cost per synthesis-and-characterization experiment in alloy and crystal materials research, these savings represent not only a methodological advance but a tangible reduction in the financial and human cost of materials discovery — accelerating the path from hypothesis to optimized material across a wide range of technologically important material classes.

5 Data and Code Availability

The Cu-alloy and glass-forming alloy datasets are publicly available from the repositories reported in their respective references [53, 57]. The LTC dataset will be made available upon reasonable request to the corresponding author. Source code for reproducing all experiments will be released openly at the project’s GitHub repository upon publication.

6 Contribution

Conceptualization, J.F.H.; methodology, J.F.H., J.H., R.D., Y.F., C.W.; software, J.F.H., J.H., R.D., Y.F.; resources, J.H.; writing—original draft preparation, J.F.H., J.H., R.D., Y.F., C.W.; writing—review and editing, J.H.; visualization, J.H., Y.F., and R.D.; supervision, J.H.; funding acquisition, J.H.

References

- [1] Turab Lookman, Prasanna V. Balachandran, Dezheng Xue, and Ruihao Yuan. Active learning in materials science with emphasis on adaptive sampling using uncertainties for targeted design. *npj Computational Materials*, 5:21, 2019.

- [2] Turab Lookman, YuJie Liu, and Zhibin Gao. Materials informatics: Emergence to autonomous discovery in the age of ai. *Advanced Materials*, page e15941, 2026.
- [3] Jiaxin Chen, Tianjiao Wan, Hui Geng, Liang Xiong, Guohong Wang, Yihan Zhao, Longxiang Deng, Susu Fang, Zheng Luo, Huaimin Wang, et al. A survey of active learning in materials science: Data-driven paradigm for accelerating the research pipeline. *arXiv preprint arXiv:2601.06971*, 2026.
- [4] Mojan Omidvar, Hangfeng Zhang, Achintha Avin Ihalage, Theo Graves Saunders, Henry Giddens, Michael Forrester, Sajad Haq, and Yang Hao. Accelerated discovery of perovskite solid solutions through automated materials synthesis and characterization. *Nature Communications*, 15:7980, 2024.
- [5] Gang Wang, Shinya Mine, Duotian Chen, Yuan Jing, Kah Wei Ting, Taichi Yamaguchi, Motoshi Takao, Zen Maeno, Ichigaku Takigawa, Koichi Matsushita, Ken-ichi Shimizu, and Takashi Toyao. Accelerated discovery of multi-elemental reverse water-gas shift catalysts using extrapolative machine learning approach. *Nature Communications*, 14:5861, 2023.
- [6] Junseok Moon, Wiktor Beker, Marta Siek, Jiheon Kim, Hyeon Seok Lee, Taeghwan Hyeon, and Bartosz A. Grzybowski. Active learning guides discovery of a champion four-metal perovskite oxide for oxygen evolution electrocatalysis. *Nature Materials*, 23:108–115, 2024.
- [7] Juran Noh, Hieu A. Doan, Heather M. Job, Lily A. Robertson, Lu Zhang, Rajeev S. Assary, Karl T. Mueller, Vijayakumar Murugesan, and Yangang Liang. An integrated high-throughput robotic platform and active learning approach for accelerated discovery of optimal electrolyte formulations. *Nature Communications*, 15:2757, 2024.
- [8] Burr Settles. Active learning literature survey. 2009.
- [9] Rui Ding, Jianguo Liu, Kang Hua, Xuebin Wang, Xiaoben Zhang, Minhua Shao, Yuxin Chen, and Junhong Chen. Leveraging data mining, active learning, and domain adaptation for efficient discovery of advanced oxygen evolution electrocatalysts. *Science Advances*, 11(14):eadr9038, 2025.
- [10] Ruihao Yuan, Zhen Liu, Prasanna V Balachandran, Deqing Xue, Yumei Zhou, Xiangdong Ding, Jun Sun, Dezhen Xue, and Turab Lookman. Accelerated discovery of large electrostrains in batio₃-based piezoelectrics using active learning. *Advanced materials*, 30(7):1702884, 2018.
- [11] Lindsay Bassman Oftelie, Pankaj Rajak, Rajiv K Kalia, Aiichiro Nakano, Fei Sha, Jifeng Sun, David J Singh, Muratahan Aykol, Patrick Huck, Kristin Persson, et al. Active learning for accelerated design of layered materials. *npj Computational Materials*, 4(1):74, 2018.
- [12] Manu Suvarna, Tangsheng Zou, Sok Ho Chong, Yuzhen Ge, Antonio J. Martín, and Javier Pérez-Ramírez. Active learning streamlines development of high performance catalysts for higher alcohol synthesis. *Nature Communications*, 15:5844, 2024.
- [13] Minki Kim, Min Young Ha, Woo-Bin Jung, Jeeseo Yoon, Euichul Shin, Il-doo Kim, Won Bo Lee, YongJoo Kim, and Hee-tae Jung. Searching for an optimal multi-metallic alloy catalyst by active learning combined with experiments. *Advanced Materials*, 34(19):2108900, 2022.
- [14] Ziyuan Rao, Po-Yen Tung, Ruiwen Xie, Ye Wei, Hongbin Zhang, Alberto Ferrari, Peter Klaver, Fritz Körmann, Prithiv T Sukumar, Alisson K da Silva, et al. Machine learning-enabled high-entropy alloy discovery. *Science*, 378(6615):78–85, 2022.
- [15] Christian Kunkel, Johannes T Margraf, Ke Chen, Harald Oberhofer, and Karsten Reuter. Active discovery of organic semiconductors. *Nature Communications*, 12(1):2422, 2021.
- [16] Gary Tom, Stefan P Schmid, Sterling G Baird, Yang Cao, Kourosh Darvish, Han Hao, Stanley Lo, Sergio Pablo-García, Ella M Rajaonson, Marta Skreta, et al. Self-driving laboratories for chemistry and materials science. *Chemical Reviews*, 124(16):9633–9732, 2024.
- [17] Richard B Canty, Jeffrey A Bennett, Keith A Brown, Tonio Buonassisi, Sergei V Kalinin, John R Kitchin, Benji Maruyama, Robert G Moore, Joshua Schrier, Martin Seifrid, et al. Science acceleration and accessibility with self-driving labs. *Nature Communications*, 16(1):3856, 2025.
- [18] Nathan J. Szymanski, Bernardus Rendy, Yuxing Fei, Rishi E. Kumar, Tanjin He, David Milsted, Matthew J. McDermott, Max Gallant, Ekin Dogus Cubuk, Amil Merchant, Haegyeom Kim, Anubhav Jain, Christopher J. Bartel, Kristin Persson, Yan Zeng, and Gerbrand Ceder. An autonomous laboratory for the accelerated synthesis of novel materials. *Nature*, 624(7990):86–91, 2023.
- [19] Milad Abolhasani and Eugenia Kumacheva. The rise of self-driving labs in chemical and materials sciences. *Nature Synthesis*, 2(6):483–492, 2023.
- [20] Christopher Tosh, Mauricio Tec, Jessica B White, Jeffrey F Quinn, Glorymar Ibanez Sanchez, Paul Calder, Andrew L Kung, Filemon S Dela Cruz, and Wesley Tansey. A bayesian active learning platform for scalable combination drug screens. *Nature Communications*, 16(1):156, 2025.

- [21] Egor Marin, Margarita Kovaleva, Maria Kadukova, Khalid Mustafin, Polina Khorn, Andrey Rogachev, Alexey Mishin, Albert Guskov, and Valentin Borshchevskiy. Regression-based active learning for accessible acceleration of ultra-large library docking. *Journal of Chemical Information and Modeling*, 64(7):2612–2623, 2024.
- [22] Hanhwi Jang, Wooseok Lee, Hwa-Jung Kim, Sohyang Cha, Hosun Shin, Won Bo Lee, Min-Wook Oh, Yeon Sik Jung, and YongJoo Kim. Active learning-guided accelerated discovery of ultra-efficient high-entropy thermoelectrics. *Advanced Materials*, page e2515054, 2025.
- [23] A. Gilad Kusne, Heshan Yu, Chenghao Wu, Hao Zhang, Jason Hattrick-Simpers, Brian DeCost, Suchismita Sarker, Corey Oses, Cormac Toher, Stefano Curtarolo, Albert V. Davydov, Ritchie Auyeung, Apurva Mehta, Arie Zaban, and Ichiro Takeuchi. On-the-fly closed-loop materials discovery via Bayesian active learning. *Nature Communications*, 11:5966, 2020.
- [24] Peiyuan Ma, Ritesh Kumar, Ke-Hsin Wang, and Chibueze V. Amanchukwu. Active learning accelerates electrolyte solvent screening for anode-free lithium metal batteries. *Nature Communications*, 16:8396, 2025.
- [25] Lars Kotthoff, Hud Wahab, and Patrick Johnson. Bayesian optimization in materials science: a survey. *arXiv preprint arXiv:2108.00002*, 2021.
- [26] Qiaohao Liang, Aldair E Gongora, Zekun Ren, Armi Tiihonen, Zhe Liu, Shijing Sun, James R Deneault, Daniil Bash, Flore Mekki-Berrada, Saif A Khan, Kedar Hippalgaonkar, Benji Maruyama, Keith A. Brown, John Fisher III, and Tonio Buonassisi. Benchmarking the performance of bayesian optimization across multiple experimental materials science domains. *npj Computational Materials*, 7(1):188, 2021.
- [27] Ahmed Shoyeb Raihan, Hamed Khosravi, Srinjoy Das, and Imtiaz Ahmed. Accelerating material discovery with a threshold-driven hybrid acquisition policy-based bayesian optimization. *Manufacturing Letters*, 41:1300–1311, 2024.
- [28] Fuhao Ji, Auralee Edelen, Ryan Roussel, Xiaozhe Shen, Sara Miskovich, Stephen Weathersby, Duan Luo, Mianzhen Mo, Patrick Kramer, Christopher Mayes, et al. Multi-objective bayesian active learning for mev-ultrafast electron diffraction. *Nature Communications*, 15(1):4726, 2024.
- [29] Ziyuan Rao and Anurag Bajpai. Active learning strategies for the design of sustainable alloys. *Philosophical Transactions of the Royal Society A*, 382(2284):20230242, 2024.
- [30] C Wang et al. Accelerated discovery of high-performance al-si-mg-sc casting alloys by integrating active learning with high-throughput calphad calculations. *Acta Materialia*, 231:117869, 2022.
- [31] Jeong Ah Lee, Jaeyung Park, Man Jae Sagong, Soung Yeoul Ahn, Jung-Wook Cho, Seungchul Lee, and Hyoung Seop Kim. Active learning framework to optimize process parameters for additive-manufactured ti-6al-4v with high strength and ductility. *Nature Communications*, 16(1):931, 2025.
- [32] Sk Md Ahnaf Akif Alvi, Jan Janssen, Danial Khatamsaz, Danny Perez, Douglas Allaire, and Raymundo Arroyave. Hierarchical gaussian process-based bayesian optimization for materials discovery in high entropy alloy spaces. *arXiv preprint arXiv:2410.04314*, 2024.
- [33] Sk Md Ahnaf Akif Alvi, Brent Vela, Vahid Attari, Jan Janssen, Danny Perez, Douglas Allaire, and Raymundo Arróyave. Deep gaussian process-based cost-aware batch bayesian optimization for complex materials design campaigns. *arXiv preprint arXiv:2509.14408*, 2025.
- [34] Nathan S Johnson, Aashwin Ananda Mishra, Dylan J Kirsch, and Apurva Mehta. Active learning for rapid targeted synthesis of compositionally complex alloys. *Materials*, 17(16):4038, 2024.
- [35] William Trehern et al. Data-driven shape memory alloy discovery using artificial intelligence materials selection (aims) framework. *Acta Materialia*, 228:117751, 2022.
- [36] Bin Cao, Jie Xiong, Jiakuan Ma, Yuan Tian, Yirui Hu, Mengwei He, Longhan Zhang, Jiayu Wang, Jian Hui, Li Liu, et al. Bgolearn: a unified bayesian optimization framework for accelerating materials discovery. *arXiv preprint arXiv:2601.06820*, 2026.
- [37] Yue Liu, Zhengwei Yang, Xinxin Zou, Shuchang Ma, Dahui Liu, Maxim Avdeev, and Siqi Shi. Data quantity governance for machine learning in materials science. *National Science Review*, 10(7):nwad125, 2023.
- [38] Ashley S Dale, Kangming Li, Brian DeCost, Hao Wan, Yuchen Han, Yao Fehlis, and Jason Hattrick-Simpers. When active learning fails, uncalibrated out of distribution uncertainty quantification might be the problem. *arXiv preprint arXiv:2511.17760*, 2025.
- [39] Gaurav Deshmukh, Noah J Wichrowski, Nikolaos Evangelou, et al. Active learning of ternary alloy structures and energies. *Journal of Chemical Physics*, 157:000000, 2022. (Also available as OSTI Technical Report).
- [40] Ying Zhang and Chen Ling. A strategy to apply machine learning to small datasets in materials science. *Npj Computational Materials*, 4(1):25, 2018.

- [41] Pengcheng Xu, Xiaobo Ji, Minjie Li, and Wencong Lu. Small data machine learning in materials science. *npj Computational Materials*, 9(1):42, 2023.
- [42] Qionghua Zhou, Xinyu Chen, and Jinlan Wang. Machine learning assisted material discovery: A small data approach. *Accounts of Materials Research*, 6(6):685–694, 2025.
- [43] Noah Hollmann, Samuel Müller, Lennart Purucker, Arjun Krishnakumar, Max Körner, and Frank Hutter. TabPFN v2: Improved in-context learning for tabular data. *arXiv preprint arXiv:2501.02945*, 2025.
- [44] Qinyang Li, Rongzhi Dong, Nicholas Miklaucic, Jeffrey Hu, Sadman Sadeed Omeed, Lai Wei, Sourin Dey, Ming Hu, and Jianjun Hu. In context learning foundation models for materials property prediction with small datasets. *arXiv preprint arXiv:2601.00133*, 2025.
- [45] Chun-Teh Chen and Grace X Gu. Generative deep neural networks for inverse materials design using backpropagation and active learning. *Advanced Science*, 7(5):1902607, 2020.
- [46] Mohammad Javad Akbari. Machine learning-driven design and discovery of high-entropy alloys: A critical review of recent advances and future perspectives. *Metals and Materials International*, pages 1–19, 2025.
- [47] Xiaotian Xu, He Zhongping, Zheng Kaiyuan, Che Lun, and Wei Feng. Applications of machine learning in high-entropy alloys: Phase prediction, performance optimization, and compositional space exploration. *Metals*, 15(12):1349, 2025.
- [48] Brent Garrett Vela. *Gaussian Processes with Physics-Informed Prior Mean Functions for Bayesian Design of Refractory High Entropy Alloys*. PhD thesis, 2025.
- [49] Yuan Tian, Tongtong Li, Jianbo Pang, Yumei Zhou, Dezhen Xue, Xiangdong Ding, and Turab Lookman. Materials design with target-oriented bayesian optimization. *npj Computational Materials*, 11(1):209, 2025.
- [50] Sk Md Ahnaf Akif Alvi, Jan Janssen, Danial Khatamsaz, Danny Perez, Douglas Allaire, and Raymundo Arróyave. Hierarchical gaussian process-based bayesian optimization for materials discovery in high entropy alloy spaces. *Acta Materialia*, 289:120908, 2025.
- [51] Y Zhang et al. Active learning-enabled the discovery of ultra-high saturation magnetization soft magnetic alloys. *Scripta Materialia*, 257:116485, 2025.
- [52] Logan Ward, Alexander Dunn, Alireza Faghaninia, Nils ER Zimmermann, Saurabh Bajaj, Qi Wang, Joseph Montoya, Jiming Chen, Kyle Bystrom, Maxwell Dylla, et al. Matminer: An open source toolkit for materials data mining. *Computational Materials Science*, 152:60–69, 2018.
- [53] Stéphane Gorsse, Mohamed Gouné, Wei-Chih Lin, and Lionel Girard. Dataset of mechanical properties and electrical conductivity of copper-based alloys. *Scientific Data*, 10(1):504, 2023.
- [54] Renato Dario Bashualdo Bobadilla, Marcello Baricco, and Mauro Palumbo. Machine learning-driven prediction of glass-forming ability in fe-based bulk metallic glasses using thermophysical features and data augmentation. *Metals*, 15(7):763, 2025.
- [55] Xiangru Tang, Howard Dai, Elizabeth Knight, Fang Wu, Yunyang Li, Tianxiao Li, and Mark Gerstein. A survey of generative AI for de novo drug design: new frontiers in molecule and protein generation. *Briefings in Bioinformatics*, 25(4):bbae338, 2024.
- [56] Brian Rohr, Helge S Stein, Dan Guevarra, Yu Wang, Joel A Haber, Muratahan Aykol, Santosh K Suram, and John M Gregoire. Benchmarking the acceleration of materials discovery by sequential learning. *Chemical science*, 11(10):2696–2706, 2020.
- [57] Renato Dario Bashualdo Bobadilla, Marcello Baricco, and Mauro Palumbo. Machine learning-driven prediction of glass-forming ability in fe-based bulk metallic glasses using thermophysical features and data augmentation. *Metals*, 15(7):763, 2025.